Electronic Supplementary Information (ESI) for Journal of Materials Chemistry C.
This journal is © The Royal Society of Chemistry 2024

Electronic Supporting Information

Reversible Modulation of Critical Electric Fields for Field-Induced Ferroelectric Effect with Field-Cycling in ZrO_2 Thin Films †

Jonghoon Shin,[a] Dong Hoon Shin,[a] Kyung Do Kim,[a] Haengha Seo,[a] Kun Hee Ye,[ab] Jeong Woo Jeon,[a] Tae Kyun Kim,[a] Heewon Paik,[a] Haewon Song,[a] Suk Hyun Lee,[a] Jung-Hae Choi,[b] and Cheol Seong Hwang*[a]

a Department of Materials Science and Engineering, and Inter-University Semiconductor Research Center, Seoul National University, Seoul, 08826, Republic of Korea. E-mail: cheolsh@snu.ac.kr

b Center for Electronic Materials, Korea Institute of Science and Technology, Seoul, 02792, Republic of Korea

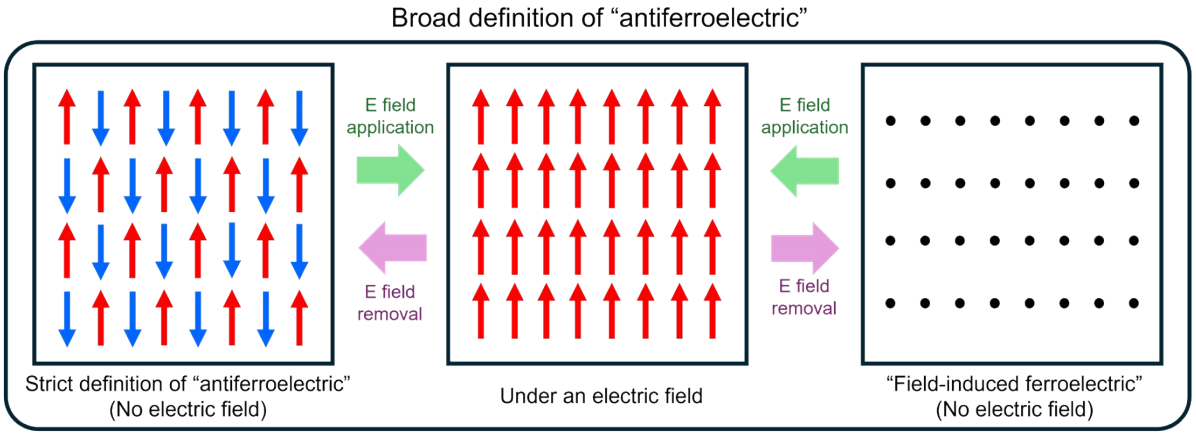

Fig. S1 Schematic diagram illustrating the difference between AFE properties, characterized by antiparallel dipoles, and FFE properties, where electric dipoles are absent without an electric field.

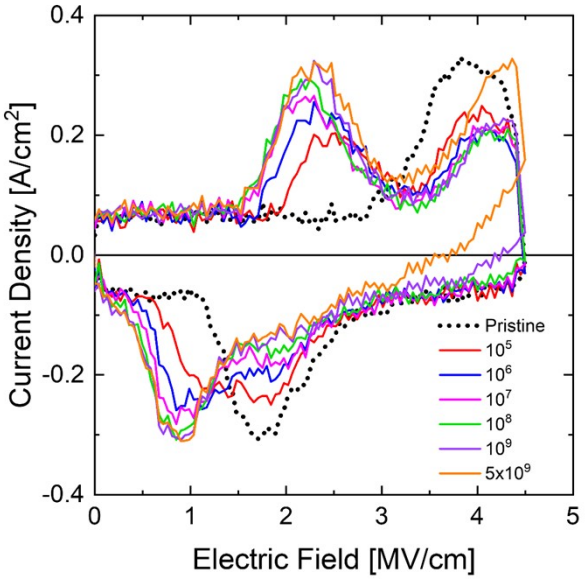

Fig. S2 I-E curve changes with field-cycling at 3.5 MV cm^{-1} for 5 x 10^9 cycles.

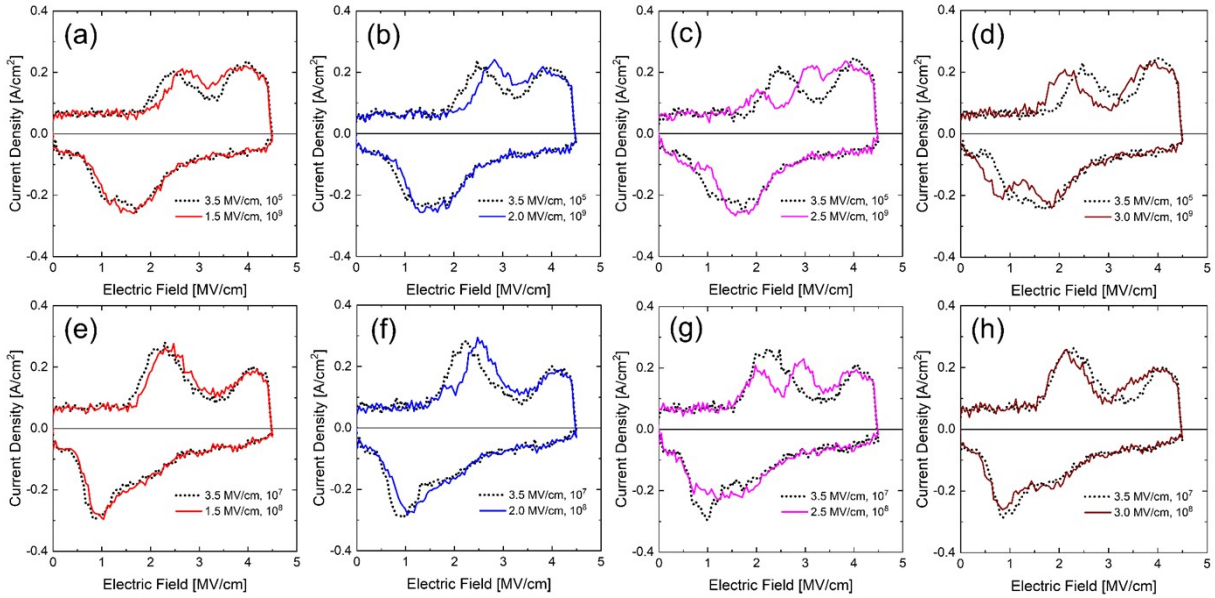

Fig. S3 I-E curves after cycling at 3.5 MV cm^{-1} for 10^5 cycles followed by 10^9 cycles at (a) 1.5 MV cm^{-1}, (b) 2.0 MV cm^{-1}, (c) 2.5 MV cm^{-1}, and (d) 3.0 MV cm^{-1}. I-E curves after cycling at 3.5 MV cm^{-1} for 10^7 cycles followed by 10^8 cycles at (e) 1.5 MV cm^{-1}, (f) 2.0 MV cm^{-1}, (g) 2.5 MV cm^{-1}, and (h) 3.0 MV cm^{-1}.

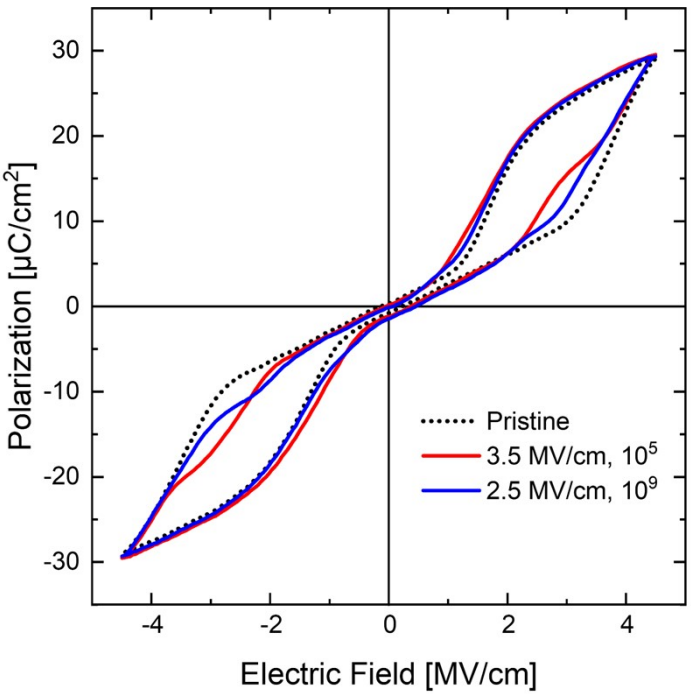

Fig. S4. P-E curves at the pristine state (dotted black) after cycling at 3.5 MV cm^{-1} for 10^5 cycles (red), and subsequent cycling at 2.5 MV cm^{-1} for 10^9 cycles (blue).

Only the critical electric fields change with higher (3.5 MV cm^{-1}) and lower (2.5 MV cm^{-1}) field cycling, whereas the $2P_r$ values exhibit minimal changes without noticeable wake-up. This result implies that the t-phase remains stable after the field-cycling without a permanent transition to the PO-phase.[1,2]

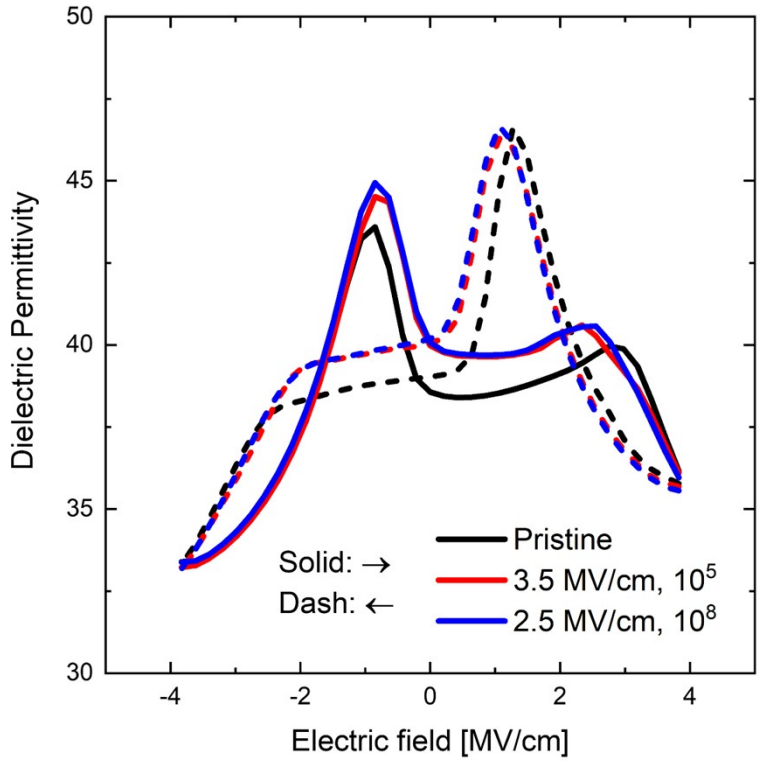

Fig. S5. *k*-E curves at the pristine state (black), after cycling at 3.5 MV cm^{-1} for 10^5 cycles (red), and subsequent cycling at 2.5 MV cm^{-1} for 10^8 cycles (blue).

The changes in the *k* values at the two ends of the *k*-E curve with field-cycling indicate the phase transition.[1,3] Minimal changes in the *k* values (~33-37) at both ends confirm that no significant phase transitions occurred after the field-cycling.[1,3]

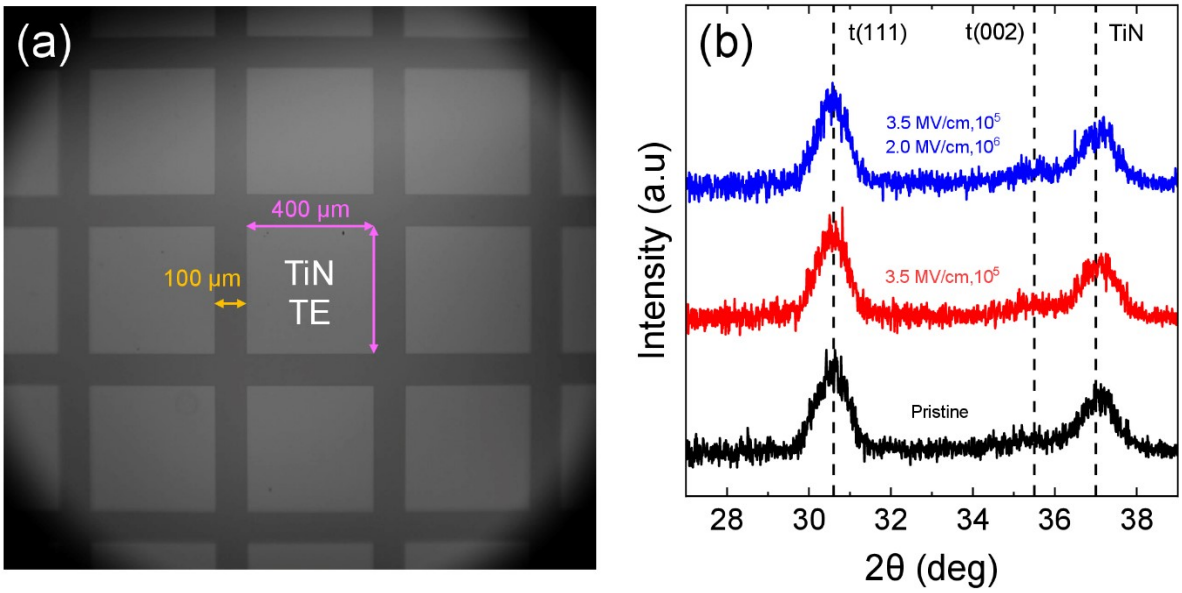

Fig. S6 (a) The optical microscope image of the sample fabricated to increase the area of the cycled capacitors relative to the total sample area. (b) Background-subtracted GIXRD patterns of the 9.4 nm ZrO_2 film at the pristine state (black), after cycling at 3.5 MV cm^{-1} for 10^5 cycles (red) and subsequent cycling at 2.0 MV cm^{-1} for 10^6 cycles (blue). All capacitors in the sample were cycled identically at each step to maximize portions of the sample affected by cycling.

Previous studies reported that the field-cycling influences the structural evolution of fluorite-structured HfO_2- or ZrO_2-based thin films.[1,4] However, directly observing the structural evolutions in cycled capacitors presents significant challenges. For instance, Cheng et al. used HAADF-STEM to detect shifts in oxygen atomic columns during cycling in HZO films.[4] However, such advanced imaging techniques are beyond the scope of this work. Therefore, structural changes induced by cycling were observed using GIXRD analysis.

Fig. S6(a) shows the optical microscope image of the sample designed for observing structural evolutions using GIXRD. For structural changes to be detectable by GIXRD, a sufficiently large sample area should consist of cycled capacitors.[5] To minimize the area not covered by the TEs, closely spaced square TEs were patterned, and all capacitors in the sample

were cycled before GIXRD measurements. The fabrication process is detailed in the Experimental Section.

Fig. S6(b) shows the background-subtracted GIXRD patterns of the 9.4 nm ZrO_2 film at different cycling states. In the pristine state (black), distinct tetragonal (111) and minor tetragonal (002) peaks appear at ~30.6° and ~35.6°, respectively. After cycling all capacitors at 3.5 MV cm^{-1} for 10^5 cycles (red) and subsequently at 2.0 MV cm^{-1} for 10^6 cycles (blue), the same peaks were observed with minimal changes, aligning with the minimal wake-up and *k* variations in Fig. S4 and S5, respectively.

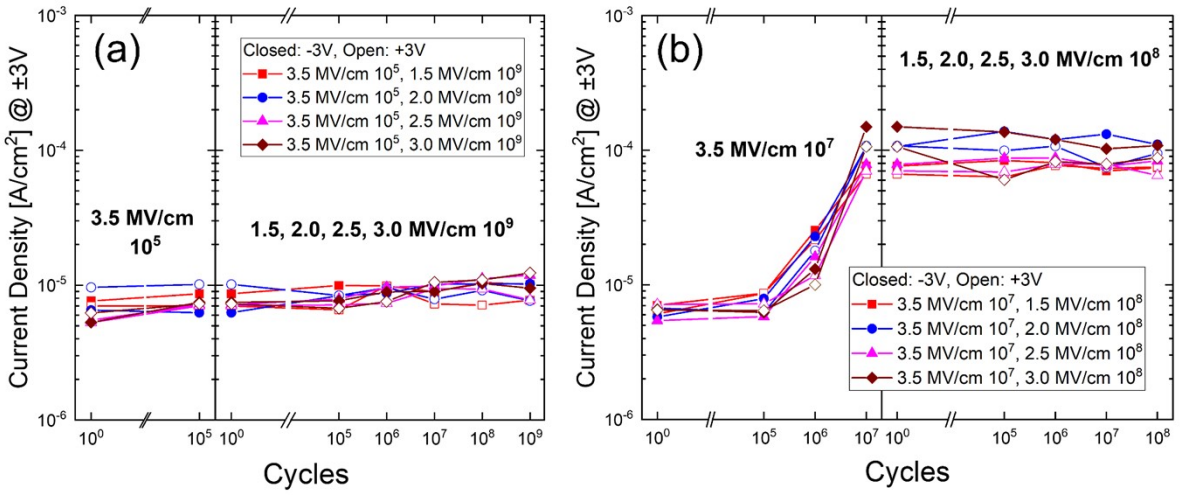

Fig. S7 Leakage current density changes at ±3V, with changing cycles for (a) cycling at 3.5 MV cm^{-1} for 10^5 cycles, followed by cycling at 1.5 / 2.0 / 2.5 / 3.0 MV cm^{-1} for 10^9 cycles, and (b) cycling at 3.5 MV cm^{-1} for 10^7 cycles, followed by cycling at 1.5 / 2.0 / 2.5 / 3.0 MV cm^{-1} for 10^8 cycles.

Previous studies on fluorite-structured HfO_2- or ZrO_2-based thin films indicated that field-cycling properties are influenced by defect chemistry.[1,4] Accurately observing defect redistribution or generation for cycled capacitors under typical laboratory conditions is challenging. However, it was suggested that changes in leakage current density could indicate defect generation in the dielectric layer with cycling.[1,4] It was elucidated in section 2-3 of the main text that the critical electric fields could change reversibly with high-field (3.5 MV cm^{-1}) and lower-field (1.5 / 2.0 / 2.5 / 3.0 MV cm^{-1}) cycling. To investigate whether the reversible changes were influenced by defect concentration, leakage current density changes with cycling were observed.

Fig. S7(a) shows the leakage current density at ±3 V after cycling at 3.5 MV cm^{-1} for 10^5 cycles, followed by 10^9 cycles at 1.5 / 2.0 / 2.5 / 3.0 MV cm^{-1}, corresponding to Fig. 6(a) of the main text. Minimal changes in leakage current density were observed in all cases, indicating that the reversible changes in Fig. 6(a) were not due to defect concentration changes. Fig. S7(b) shows the leakage current density at ±3 V after cycling at 3.5 MV cm^{-1} for 10^7 cycles, followed by 10^8 cycles at 1.5 / 2.0 / 2.5 / 3.0 MV cm^{-1}, corresponding to Fig. 6(b) of the main text. The leakage current density gradually increased after 10^6 cycles for the 3.5 MV cm^{-1} cycling case due to the high-field cycling stress[8], but subsequent lower-field cycling resulted in minimal changes. These results suggested irreversible defect generation with higher-field cycling, which remained during subsequent lower-field cycling. Hence, defect concentration change

may not be the primary cause of the reversible changes observed in Fig. 6(b).

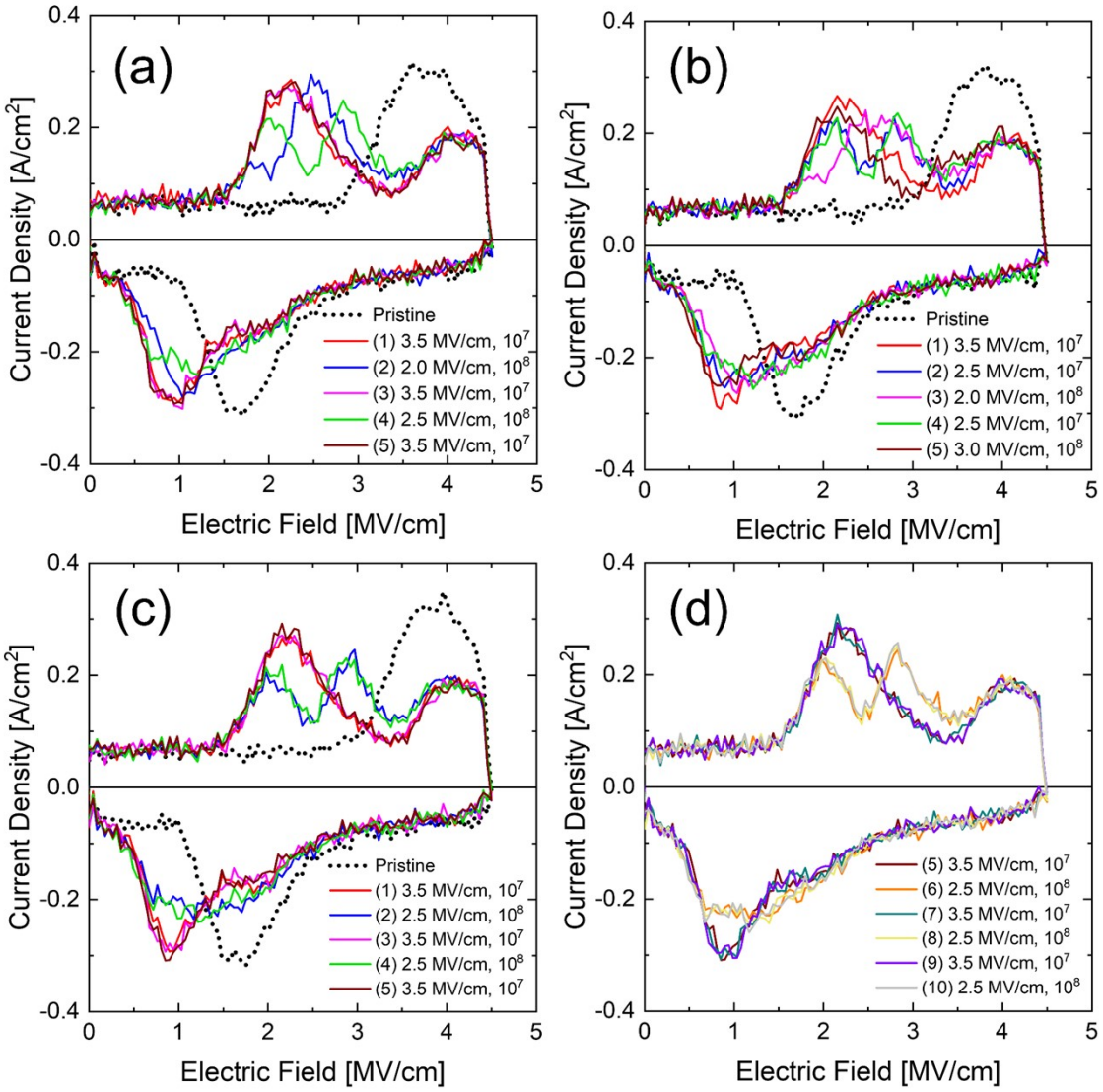

Fig. S8 (a) Sequential I-E curve changes after cycling at (1) 3.5 MV cm^{-1}, 10^7 cycles (red) → (2) 2.0 MV cm^{-1}, 10^8 cycles (blue) → (3) 3.5 MV cm^{-1}, 10^7 cycles (pink) → (4) 2.5 MV cm^{-1}, 10^8 cycles (green) → (5) 3.5 MV cm^{-1}, 10^7 cycles (brown). (b) Sequential I-E curve changes after cycling at (1) 3.5 MV cm^{-1}, 10^7 cycles (red) → (2) 2.5 MV cm^{-1}, 10^7 cycles (blue) → (3) 2.0 MV cm^{-1}, 10^8 cycles (pink) → (4) 2.5 MV cm^{-1}, 10^7 cycles (green) → (5) 3.0 MV cm^{-1}, 10^8

cycles (brown). Sequential I-E curve changes after alternating cycling of 3.5 MV cm^{-1} for 10^7 cycles and 2.5 MV cm^{-1} for 10^8 cycles, repeated five times, divided into (c) and (d).

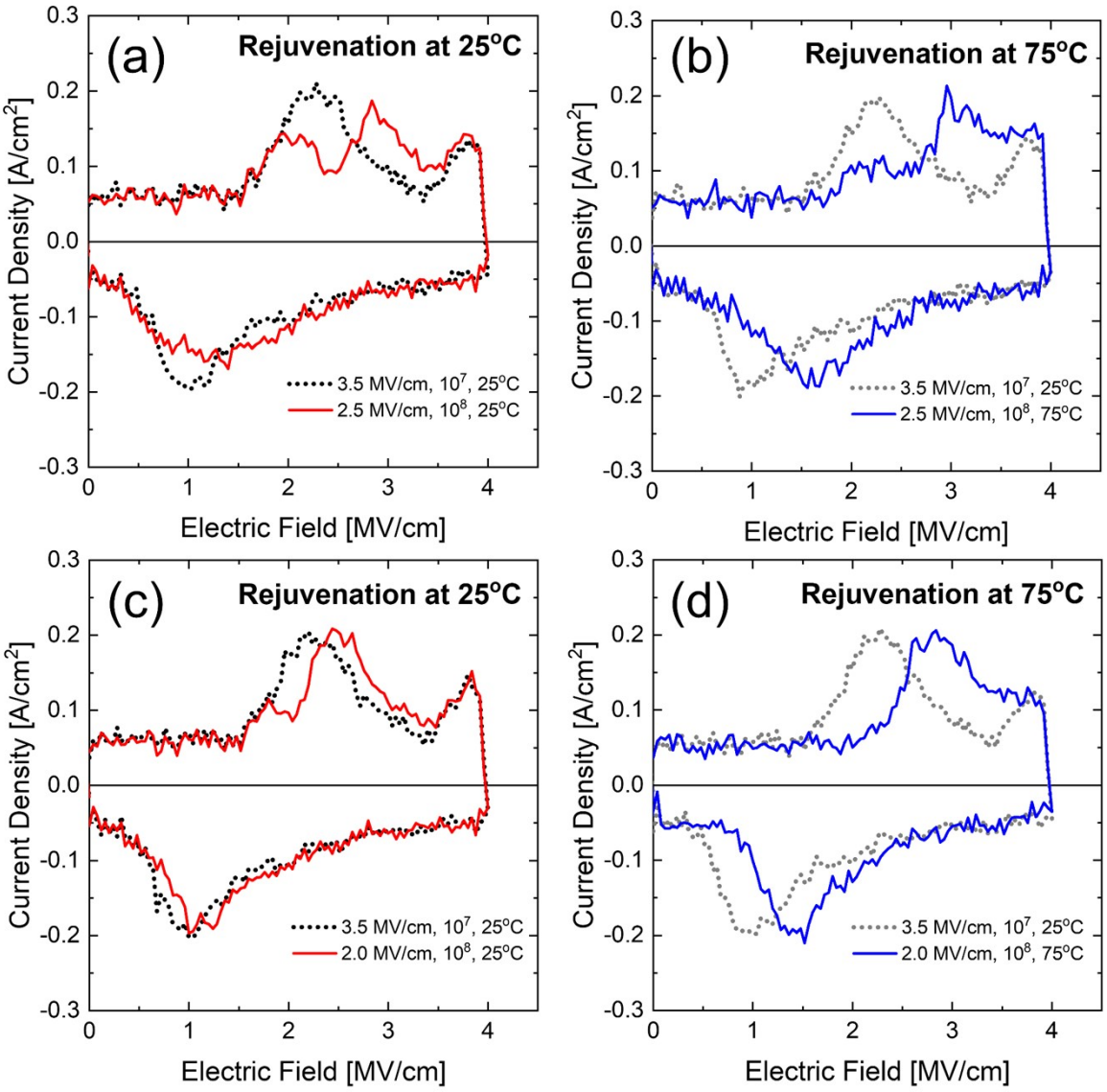

Fig. S9 I-E curves after cycling at 3.5 MV cm^{-1} for 10^7 cycles at 25°C, followed by 10^8 cycles at 2.5 MV cm^{-1} for (a) 25°C and (b) 75°C. I-E curves after cycling at 3.5 MV cm^{-1} for 10^7 cycles at 25°C, followed by 10^8 cycles at 2.0 MV cm^{-1} for (c) 25°C and (d) 75°C.

Notes and references

1. M. Pešić, F. P. G. Fengler, L. Larcher, A. Padovani, T. Schenk, E. D. Grimley, X. Sang, J. M. LeBeau, S. Slesazeck and U. Schroeder, *Adv. Funct. Mater.*, 2016, **26**, 4601-4612.
2. M. H. Park, H. J. Kim, Y. J. Kim, Y. H. Lee, T. Moon, K. D. Kim, S. D. Hyun, F. P. G. Fengler, U. Schroeder and C. S. Hwang, ACS Appl. Mater. Interfaces, 2016, **8**, 15466–15475.
3. E. D. Grimley, T. Schenk, X. Sang, M. Pešić, U. Schroeder, T. Mikolajick and J. M. LeBeau, *Adv. Electron. Mater.*, 2016, **2**, 1600173.
4. Y. Cheng, Z. M. Gao, K. H. Ye, H. W. Park, Y. H. Zheng, Y. Z. Zheng, J. F. Gao, M. H. Park, J. H. Choi, K. H. Xue, C. S. Hwang and H. B. Lyu, *Nat. Commun*, 2022, **13**.
5. S. Nittayakasetwat, H. Momiyama and K. Kita, *Solid-State Electron.*, 2023, **204**, 108639.
6. G. H. Park, D. H. Lee, H. Choi, T. Kwon, Y. H. Cho, S. H. Kim and M. H. Park, *ACS Appl. Electron. Mater.*, 2023, **5**, 642-663.
7. M. H. Park and C. S. Hwang, *Rep. Prog. Phys.*, 2019, **82**, 124502.
8. S. D. Hyun, H. W. Park, M. H. Park, Y. H. Lee, Y. B. Lee, B. Y. Kim, H. H. Kim, B. S. Kim and C. S. Hwang, *Adv. Electron. Mater.*, 2020, **6**, 2000631.